analytical chemistry

Letter

pubs.acs.org/ac

High-Speed Multiparameter Photophysical Analyses of Fluorophore Libraries

Kevin M. Dean,[†,‡] Lloyd M. Davis,[§,∥] Jennifer L. Lubbeck,[‡,⊥] Premashis Manna,[‡,⊥] Pia Friis,[‡,⊥] Amy E. Palmer,*[,†,‡] and Ralph Jimenez*[,‡,⊥]

[†]BioFrontiers Institute, University of Colorado, Boulder, Colorado 80309, United States

[‡]Department of Chemistry and Biochemistry, University of Colorado, Boulder, Colorado 80309, United States

[§]Department of Physics, University of Tennessee Knoxville, Knoxville, Tennessee 37996, United States

[∥]Center for Laser Applications, University of Tennessee Space Institute, Tullahoma, Tennessee 37388, United States

[⊥]JILA, NIST, and University of Colorado, Boulder, Colorado 80309, United States

Supporting Information

ABSTRACT: There is a critical need for high-speed multiparameter photophysical measurements of large libraries of fluorescent probe variants for imaging and biosensor development. We present a microfluidic flow cytometer that rapidly assays 10^4−10^5 member cell-based fluorophore libraries, simultaneously measuring fluorescence lifetime and photobleaching. Together, these photophysical characteristics determine imaging performance. We demonstrate the ability to resolve the diverse photophysical characteristics of different library types and the ability to identify rare populations.

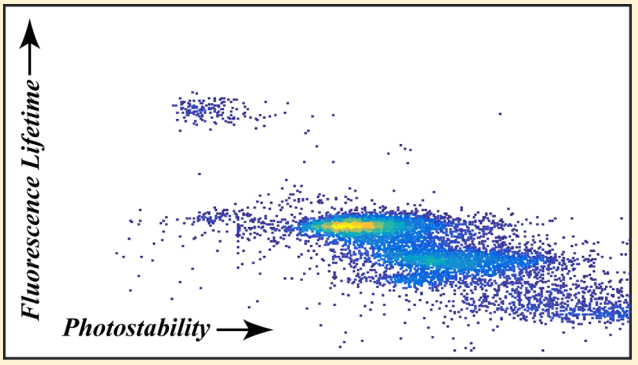

The widespread availability of combinatorial chemical and biochemical methods for generating large, diverse molecular libraries strongly motivates the development of strategies for high-throughput spectroscopic analysis. One approach includes confining the molecules of interest to micrometer-scale particles (e.g., cells).[1] However, most high-throughput analyses are restricted to fluorescence intensity-based methods. This complicates the search for new molecules with complex photophysical functionality, such as photoswitching fluorophores with improved photostability, which are needed for super-resolution imaging and other advanced photonic applications.

On the other hand, more detailed photophysical analysis typically requires purification of the molecular species, followed by experimental interrogation and detailed theoretical analysis.[2] The results for a small number of molecular scaffolds, or sequence variants of a protein or nucleic acid, are then modeled in an effort to elucidate how molecular structure dictates photophysical function within this panel.[3] Unfortunately, this approach is time-intensive and sampling a statistically sufficient number of variants to stringently evaluate a model remains an ongoing challenge. Here, we illustrate that multiple measurements can be performed in a flow environment to provide multiparameter and high-throughput optical spectroscopy. This approach is versatile and can be combined with a diverse array of optical techniques, with the duration of the interrogation per cell ($\sim 10^{-6}$−10^{0} s) controlled by the microfluidic design and flow speed.

We developed a microfluidic platform employing a multibeam pump/probe method that rapidly measures two critical parameters for the performance of a fluorophore in imaging applications: the excitation intensity-dependent fluorescence lifetime and the extent of irreversible photobleaching. The fluorescence lifetime is a sensitive indicator of radiative and nonradiative excited-state processes and yields information pertaining to the fluorescence quantum yield (Note S1, Supporting Information). Irreversible photobleaching is the permanent chemical alteration of a molecule that renders it nonfluorescent following excitation, often attributed to a reaction that proceeds from an excited singlet or triplet level to reactive radical states or transient absorption from an excited state. The rate of irreversible photobleaching yields information pertaining to the mean number of excitations that a molecule can sustain. For most applications, one seeks members of the molecular library that have both low rates of irreversible photobleaching and a high fluorescence quantum yield.

In our instrument, a fluorophore-labeled cell traversing the interrogation channel of a 2D hydrofocusing microfluidic network interacts with several spatially separated laser beams

Received: February 12, 2015
Accepted: April 21, 2015

DOI: 10.1021/acs.analchem.5b00607
Anal. Chem. XXXX, XXX, XXX−XXX

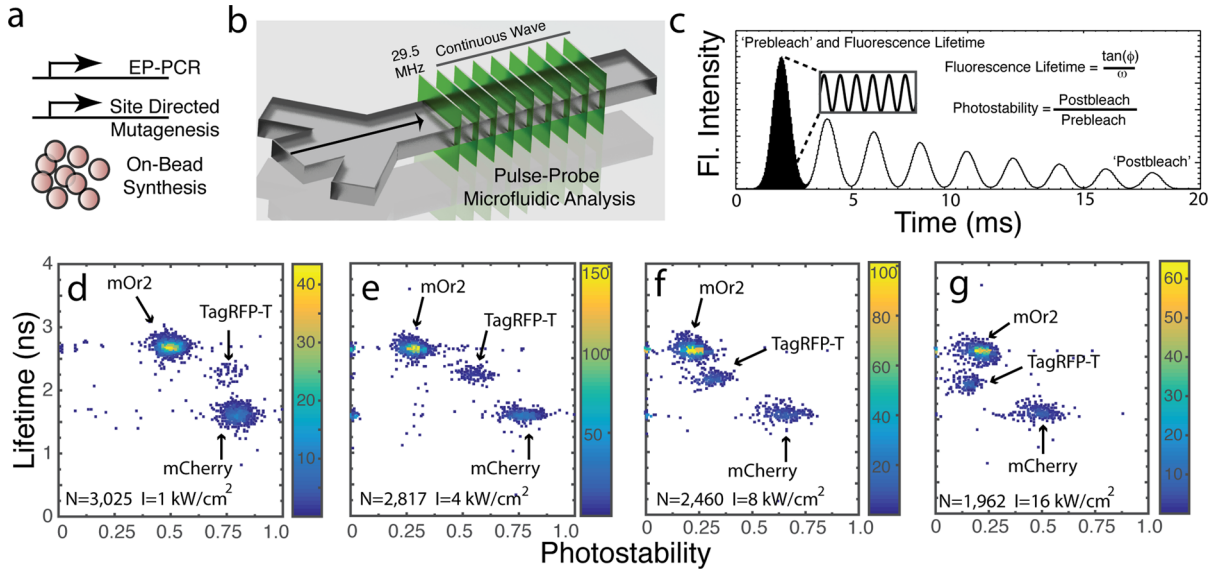

Figure 1. Schematic of the microfluidic assay for measuring fluorescence lifetime and irreversible photobleaching and intensity-dependent analysis of a three fluorescent protein mixture. (a) Spectroscopically pure molecular variants confined to micrometer-scale particles or cells are pooled and (b) hydrodynamically focused in a microfluidic device where the particles traverse a series of elliptically focused laser beams (λ = 532 nm). The first beam, modulated at 29.5 MHz, measures the fluorescence lifetime and initial particle fluorescence intensity ("prebleach"). The ninth beam measures the remaining fluorescence ("postbleach") following cycles of excitation and relaxation by the intervening beams. Excitation events are spatiotemporally resolved, and the ratio of the postbleach and prebleach signals quantitatively measures the photostability. (c) Illustration showing how the total fluorescence from the particle traversing the 9 beams consists of a series of separated pulses decaying in amplitude as the particle undergoes photobleaching. Only the first and last pulses are recorded. (d–g) Fluorescence lifetime and photostability analysis of HeLa suspension cells expressing TagRFP-T, mCherry, and mOrange2 at an excitation intensity I of (d) 1, (e) 4, (f) 8, and (g) 16 kW/cm^2. Increases in laser intensity result in reordering of the photostability ranking and gradual decreases in fluorescence lifetime for TagRFP-T and mOrange2, but changes for mCherry, which are expected to be smaller (see Figure S-3, Supporting Information), were not resolved. Color scale corresponds to the number of cells represented by each data point, and N gives the total number of cells in the sample measured for each condition. Because the arrival of cells is random and the instrument was run for different durations of time, N varies between samples.

(Figure 1a–c). The first interrogation point is a 29.5 MHz sinusoidally modulated beam, which serves as an excitation source for frequency-domain fluorescence lifetime measurements (Note S2, Supporting Information).[4] Also, the low-frequency component (<1 MHz) of fluorescence from this beam is electronically isolated, and the amplitude of the resulting signal provides the initial fluorescence intensity prior to photobleaching (hereafter called the "prebleach" signal). The cell then traverses a series of 7 separated beams that induce photobleaching and, finally, through the second analysis region, which captures the "postbleach" fluorescence intensity. The ratio of the post- to prebleach fluorescence intensities quantifies the photobleaching, independent of fluorophore density.[5] A key feature of this multibeam millisecond illumination scheme is that it permits relaxation of reversible dark states between beams, thereby isolating the irreversible photobleaching component.[5−7] Using this instrument, the fluorescence lifetime and photostability can be measured at rates up to ∼180 cells per second (Note S3, Supporting Information), thereby sampling the diversity and quantifying the correlation of fluorescence lifetime with irreversible photostability across 10^4–10^5 molecular variants, in less than 10 min.

As an initial application, we examined the dependence of fluorescence lifetime and photostability on laser intensity using a mixture of three types of HeLa suspension cells, each constitutively expressing red-fluorescent proteins (RFPs) commonly used in biological imaging, including mCherry, TagRFP-T, and mOrange2.[8−10] At an average laser intensity, I_{EX}, of 1 kW/cm^2 (measured as the laser power divided by the elliptical beam area at full width half-maximum (Note S2, Supporting Information)), three subpopulations were observed along the lifetime and photostability axes (Figure 1d). Although the measured photostability is expected to decrease with laser intensity, an unexpected reordering was observed for the different fluorophores. For example, at I_{EX} = 4–8 kW/cm^2, the mCherry population was the most photostable, followed by TagRFP-T and then mOrange2 (Figure 1e,f). However, at higher power, I_{EX} = 16 kW/cm^2, mOrange2 became more photostable than TagRFP-T (Figure 1g). As the laser intensity is increased from 1 to 16 kW/cm^2, small decreases (∼100 ps) were also observed in the measured values of the fluorescence lifetimes for mOrange2 and TagRFP-T, but not for mCherry (p < 0.001, < 0.001, and 0.055, respectively, Table S-1, Supporting Information). The decreases in the lifetimes likely arise from saturation,[11] as is modeled below. The statistical power arising from measurements on 10^3 cells enables small changes to be monitored and differences in the behavior of different fluorophores to be observed.

Next, we investigated the effect of various mutagenesis strategies on RFP photophysical output. Given the vastness of protein sequence space, directed-evolution experiments would benefit from improved diagnosis of the efficacy of the method used for molecular perturbation (e.g., error-prone vs saturated mutagenesis) and the resultant spectroscopic diversity.[12] Four libraries (Supporting Methods, Supporting Information) were screened at I_{EX} = 4 kW/cm^2, including: mCherry[8] site-directed mutagenesis, 1.44 × 10^5 mutants (Figure 2a); mRuby2[13] Error-Prone PCR (EP-PCR), 1.5 × 10^6 mutants, (Figure 2b); TagRFP-T EP-PCR, 1.4 × 10^6 mutants, (Figure 2c); and

DOI: 10.1021/acs.analchem.5b00607
Anal. Chem. XXXX, XXX, XXX−XXX

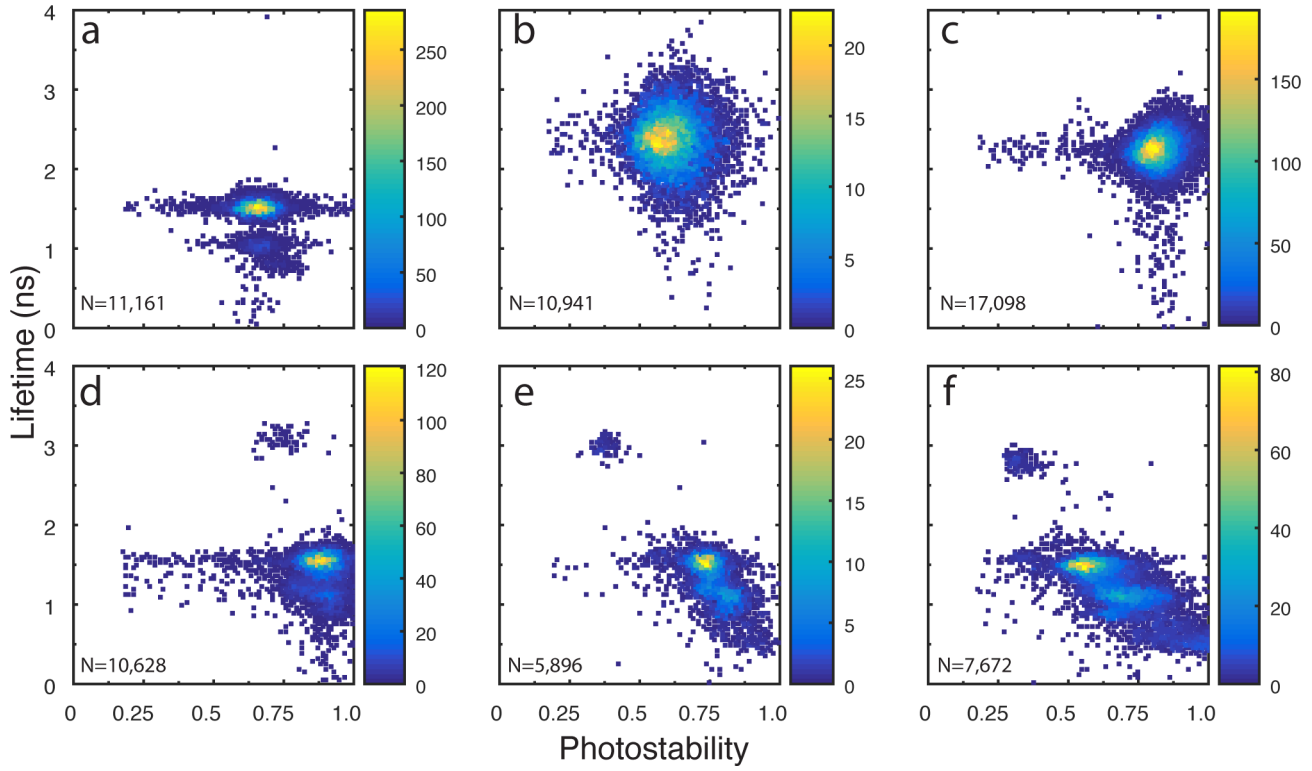

Figure 2. Photophysical diversity resulting from different mutagenic strategies. (a) mCherry semisaturated mutagenesis (positions 16, 66, 143, 161, and 163), (b) mRuby2 EP-PCR, (c) TagRFP-T EP-PCR, and (d) mCherry combined semisaturated mutagenesis and EP-PCR with an excitation intensity of 4 kW/cm^2. Excitation intensity-dependence of combined semisaturated mutagenesis and EP-PCR library with an excitation intensity of (e) 8 and (f) 16 kW/cm^2. Color scale corresponds to the number of cells represented by each data point. Because the arrival of cells is random and the instrument was run for different durations of time, *N* varies between samples.

mCherry site-directed mutagenesis coupled with EP-PCR, 2.73 × 10^6 mutants (Figure 2d).

Site-directed mutagenesis libraries consistently manifested multimodal distributions (Figure 2a,d), whereas EP-PCR libraries were unimodal and shared mean photophysical properties with the parent RFP, albeit with broadened distributions in both the lifetime and photobleaching dimensions (Figure 2b,c). Indeed, even without screening every member of each library, density-based computational clustering confirmed the presence of subpopulations in the site-directed, but not error-prone, mutagenesis libraries (Figure S-1, Supporting Information).[14] However, identifying very small populations at the level of a few cells would require complete coverage of each library. These data suggest that EP-PCR mutagenesis is less likely to drastically influence protein function. In contrast, site-directed mutagenesis at positions known to interact with the chromophore are much more likely to modulate photophysical output. Furthermore, the presence of distinct subpopulations suggests that there may be dominant mutations or combinations of mutations that trigger phenotypic switching, with supporting mutations that further tune spectroscopic output.[15] These results are analogous to those observed in molecular and biological evolution, in which the clusters of photophysical behavior correspond to diverse branches of a phylogenetic tree.[16]

We performed intensity-dependent measurements on the mCherry combined site-directed and error-prone mutagenesis library. At 4 kW/cm^2, the population was distributed along both the photostability and lifetime axes (Figure 2d). The majority of the library had a fluorescence lifetime shorter than 1.7 ns, with the exception of a small subset (2.3%) located at ∼3.1 ns. As the excitation intensity was increased from 4 to 16 kW/cm^2, the average lifetime of this subpopulation progressively decreased from 3.07 to 2.81 ns (Table S-1, Supporting Information, $p < 0.001$, Figure 2d–f). To explore the hypothesis that the observed decrease in the apparent fluorescence lifetime is an artifact resulting from ground-state depletion or saturation-induced shifts in the phase of the observed fluorescence modulation,[11] we performed excitation intensity-dependent numerical simulations on a simple two-state model consisting of a ground (S_0) and an excited state (S_1) with known parameters for the fluorophores (Figure S-2a, Supporting Information).[17] The simulations revealed that ground-state depletion reduces the phase shift and hence decreases the apparent lifetime by amounts consistent with our observations, ∼100 ps for mOrange2 and TagRFP-T and less so for mCherry (Figure S-3, Supporting Information).

Although increases in the excitation intensity decreased the photostability of the library, the decrease was nonuniform; mutants with longer fluorescence lifetimes photobleached more than those with short lifetimes. Indeed, at 16 kW/cm^2, photostability and fluorescence lifetime were inversely correlated (Figure 2f, Pearson product-moment correlation coefficient, −0.65). We investigated the relation between these parameters with simulations on a 3-state model (Figure S-2b, Supporting Information). Specifically, we sought to gauge within this library whether diversification of the fluorescence lifetime was sufficient to explain the observed changes in photostability. Simulations measured the amount of photobleaching after 9 illumination events as a function of the

DOI: 10.1021/acs.analchem.5b00607
Anal. Chem. XXXX, XXX, XXX−XXX

fluorescence lifetime, the rate of S_1-mediated photobleaching, and excitation intensity. The results of the simulations at 4 and 16 kW/cm^2 are shown in Figure 3a,b, respectively. Dashed lines represent rates of S_1-mediated photobleaching, and the mean photostabilities of the binned data from Figure 2d,f are shown as color-coded dots. Interestingly, much of these data fall onto a single curve, indicating that the library diversified the fluorescence lifetime and not the rate of photobleaching. However, some deviations are observed in the 16 kW/cm^2 model at low fluorescence lifetimes, potentially arising from poor sampling of these weakly fluorescent variants. Model sensitivity analysis suggested that the photostability was more sensitive to the excited-state lifetime than other photokinetic parameters, such as the rate of dark-state conversion, dark-state relaxation, or dark-state photobleaching (Figure S-4, Supporting Information).

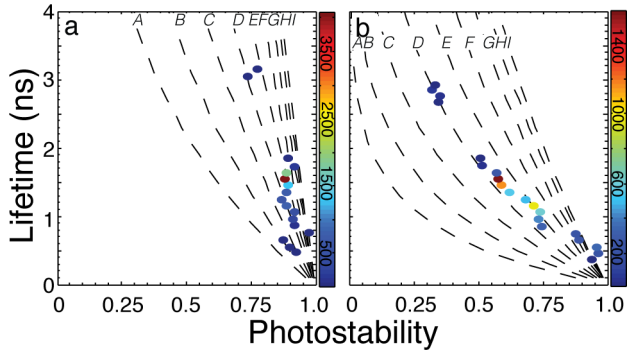

Figure 3. Multiparameter photobleaching simulations of a 3-state model. Simulation results for excitation intensities of (a) 4 and (b) 16 kW/cm^2. Lifetimes were varied from 0.2 to 5 ns, and the rate of photobleaching (k_{BL1}) from S_1 was varied: (A) 1×10^5, (B) 6×10^4, (C) 4×10^4, (D) 2.5×10^4, (E) 1.6×10^4, (F) 1.25×10^4, (G) 1×10^4, (H) 6×10^3, and (I) 4×10^3 (Hz). The average photostability as a function of lifetime for each 200 ps bin of the data (from Figure 2d,f) is plotted. Color scale corresponds to the number of cells represented by each data point.

In conclusion, we have introduced a new high-throughput multiparameter spectroscopic technique for screening large libraries of fluorescent probe variants. The technique, which involves confining the molecules of interest to micrometer-scale particles such as cells, represents a significant advance beyond methods that only rely on multiwavelength excited/detected fluorescence intensity. As such, we are the first to observe an inverse correlation between fluorescence lifetime and photostability in RFP mutants. The increased data dimensionality and statistical power enable insights unavailable from standard spectroscopy workflow, such as the identification of subpopulations and insight into how different photophysical parameters correlate across 10^4 to 10^5 molecular variants. The dimensionality of the data can be increased with additional optical interrogation points (e.g., fluorescence anisotropy, multiwavelength absorption/emission, transient absorption, or Raman measurements). Fluorescent probes can be subjected to environmental perturbations via subcellular localization or solvent mixing, for cells and beads, respectively, enabling probe analysis in unique chemical environments (e.g., reducing, oxidizing, acid–base). Following interrogation, the molecular species could be identified by mass cytometry[18] or optical sorting[5] of the particles. These capabilities will make multiparameter microfluidic cytometry a powerful tool for optical spectroscopy, chemical biology, and directed evolution.

METHODS

Detailed methods regarding the construction of fluorescent protein libraries, microfluidic chip design and operation, optics, phase-detection electronics, numerical simulations, and clustering analysis are provided in the Supporting Information.

ASSOCIATED CONTENT

Supporting Information

Detailed experimental methods, the relationship between fluorescence lifetime and fluorescence quantum yield, the theory of frequency-domain fluorescence lifetime flow cytometry, and the maximum instrument screening rate. This material is available free of charge via the Internet at http://pubs.acs.org.

AUTHOR INFORMATION

Corresponding Authors

*E-mail: amy.palmer@colorado.edu.
*E-mail: rjimenez@jila.colorado.edu.

Author Contributions

K.M.D., L.M.D., J.L.L., A.E.P, and R.J. conceived and designed the experiments. K.M.D., L.M.D., and J.L.L. built the instrument. K.M.D. and P.M. performed the experiments and numerical simulations. K.M.D. constructed the libraries, and P.F. provided technical assistance. K.M.D., L.M.D., A.E.P., and R.J. wrote the manuscript.

Notes

The authors declare no competing financial interest.

ACKNOWLEDGMENTS

We would like to thank Dr. Assaf Zaritsky (UT Southwestern Med. Ctr.) for his assistance with the clustering analysis. This work was supported by the NIH (GM083849, A.E.P. and R.J.), University of Colorado Molecular Biophysics Training Grant (T32 GM065103), NSF Computational Optical Sensing and Imaging I (0801680), and the NSF Physics Frontier Center at JILA. R.J. is a staff member of the NIST Quantum Physics Division.

REFERENCES

(1) Gerver, R. E.; Gómez-Sjöberg, R.; Baxter, B. C.; Thorn, K. S.; Fordyce, P. M.; Diaz-Botia, C. A.; Helms, B. A.; DeRisi, J. L. *Lab Chip* **2012**, *12*, 4716.
(2) Koide, Y.; Urano, Y.; Hanaoka, K.; Terai, T.; Nagano, T. *ACS Chem. Biol.* **2011**, *6*, 600–608.
(3) Subach, F. V.; Piatkevich, K. D.; Verkhusha, V. V. *Nat. Methods* **2011**, *8*, 1019–1026.
(4) Booth, M. J.; Wilson, T. *J. Microsc.* **2004**, *214*, 36–42.
(5) Davis, L. M.; Lubbeck, J. L.; Dean, K. M.; Palmer, A. E.; Jimenez, R. *Lab Chip* **2013**, *13*, 2320–2327.
(6) Dean, K. M.; Lubbeck, J. L.; Binder, J. K.; Schwall, L. R.; Jimenez, R.; Palmer, A. E. *Biophys. J.* **2011**, *101*, 961–969.
(7) Lubbeck, J. L.; Dean, K. M.; Ma, H.; Palmer, A. E.; Jimenez, R. *Anal. Chem.* **2012**, *84*, 3929–3937.
(8) Shaner, N. C.; Campbell, R. E.; Steinbach, P. A.; Giepmans, B. N.; Palmer, A. E.; Tsien, R. Y. *Nat. Biotechnol.* **2004**, *22*, 1567–1572.
(9) Shaner, N. C.; Lin, M. Z.; McKeown, M. R.; Steinbach, P. A.; Hazelwood, K. L.; Davidson, M. W.; Tsien, R. Y. *Nat. Methods* **2008**, *5*, 545–551.
(10) Merzlyak, E. M.; Goedhart, J.; Shcherbo, D.; Bulina, M. E.; Shcheglov, A. S.; Fradkov, A. F.; Gaintzeva, A.; Lukyanov, K. A.;

DOI: 10.1021/acs.analchem.5b00607
Anal. Chem. XXXX, XXX, XXX–XXX

Lukyanov, S.; Gadella, T. W. J.; Chudakov, D. M. *Nat. Methods* **2007**, *4*, 555−557.
(11) Esposito, A.; Gerritsen, H. C.; Wouters, F. S. *J. Opt. Soc. Am. A* **2007**, *24*, 3261−3273.
(12) Treynor, T. P.; Vizcarra, C. L.; Nedelcu, D.; Mayo, S. L. *Proc. Natl. Acad. Sci. U. S. A.* **2006**, *104*, 48−53.
(13) Lam, A. J.; St-Pierre, F.; Gong, Y.; Marshall, J. D.; Cranfill, P. J.; Baird, M. A.; McKeown, M. R.; Wiedenmann, J.; Davidson, M. W.; Schnitzer, M. J.; Tsien, R. Y.; Lin, M. Z. *Nat. Methods* **2012**, *9*, 1005−1012.
(14) Rodriguez, A.; Laio, A. *Science* **2014**, *344*, 1492−1496.
(15) Wang, L.; Jackson, W. C.; Steinbach, P. A.; Tsien, R. Y. *Proc. Natl. Acad. Sci. U. S. A.* **2004**, *101*, 16745−16749.
(16) Dickinson, B. C.; Leconte, A. M.; Allen, B.; Esvelt, K. M.; Liu, D. R. *Proc. Natl. Acad. Sci. U. S. A.* **2013**, *110*, 9007−9012.
(17) Manna, P.; Jimenez, R. *J. Phys. Chem. B* **2015**, *119* (15), 4944−4954.
(18) Bendall, S. C.; Simonds, E. F.; Qiu, P.; Amir, E. a. D.; Krutzik, P. O.; Finck, R.; Bruggner, R. V.; Melamed, R.; Trejo, A.; Ornatsky, O. I.; Balderas, R. S.; Plevritis, S. K.; Sachs, K.; Pe'er, D.; Tanner, S. D.; Nolan, G. P. *Science* **2011**, *332*, 687−696.

DOI: 10.1021/acs.analchem.5b00607
Anal. Chem. XXXX, XXX, XXX−XXX